2.2 Experimental Study of Thermocapillary Flow in The Half-Zone Liquid Bridge of Low Prandtl Number Fluid

NASDA Space Utilization Research Center

EXPERIMENTAL STUDY OF THERMOCAPILLARY FLOW IN THE HALF-ZONE LIQUID BRIDGE OF LOW PRANDTL NUMBER FLUID

Satoshi Matsumoto[1], Hitoshi Hayashida [1], Atsuki Komiya [1], Hidesada Natsui [2], and Shinichi Yoda [1]

[1] National Space Development Agency of Japan, 2-1-1, Sengen, Tsukuba, Ibaraki 305-8505, Japan
[2] Advanced Engineering Services Co. Ltd., 1-6-1, Takezono, Tsukuba, Ibaraki 305-0032, Japan

ABSTRACT

The experimental study on thermocapillary convection of low Prandtl number fluid was carried out to understand transition behavior to oscillatory flow. The half-zone liquid bridge of molten tin was formed between hot and cold disks in high vacuum chamber (10^{-5} Pa). The three radiation thermometers were used to measure the free surface temperature at a different azimuthal location at the same time. In addition, the temperature distribution at interface between liquid bridge and cold disk was measured by using very fine thermocouples to detect the transition point and to make clear the oscillation mode more precisely.

It can be detected that the steady thermocapillary convection changes to oscillatory under certain condition. The observed phenomena of transition processes after the oscillatory onset were revealed by comparing to numerical result done by Imaishi *et al.*. The effect of aspect ratio (L/r) on critical Marangoni number was investigated. The critical Marangoni number decreases with increasing the aspect number. This behavior agrees with numerical simulation done by Imaishi *et al.* qualitatively except for region of smaller aspect ration.

The surface tension and its temperature coefficient were measured in the experimental chamber. A molten tin droplet was formed on an α-Al_2O_3 substrate in the evacuated experimental chamber. These analog photo images were transfer to digital images and the surface tension was calculated from the outlines of digital image, which was the sessile drop method. The value of surface tension and its temperature coefficient were 520~550 [mN/m] and 0.097 [mN/m/K].

The Fe-Ni/SB tracer particle has been developed for the visualization of the inner flow pattern of the Marangoni convection. Considering the traceability of the particle, high wettability and low reactivity with surrounding fluid, and high sphericity are required. Therefore, the multi-layer structure, which comprises Fe and Ni layers, was adopted. The plating techniques of both Fe and Ni layers were developed and the heat treatment technique to make the high sphericity particles was also developed. The test particle has already been manufactured and its reflectance of ultrasonic beam has been evaluated.

1. INTRODUCTION

1. Introduction

It is well known that thermocapillary convection changes its flow motion by increasing the control parameters such as temperature difference. In the case of liquid bridge of low Prandtl number fluid, it is numerically predicted that an axisymmetric steady flow transit to asymmetric 3D steady flow. After that, convection becomes oscillatory under certain condition. Namely, the thermocapillary convection of low Prandtl number fluid go through two transition points to become an oscillatory flow. We need to understand the transition mechanism because the oscillatory flow has an undesirable effect on the crystal growth of semiconductors by the floating zone methods, which lead to striations of the dopant in the crystal. The previous studies, in which a half zone liquid bridge have been often used as a model configuration of the floating zone, have shown that flow and temperature fields were governed by dimensionless parameter of Marangoni (Ma) or Reynolds (Re) number defined as follows:

$$Ma \equiv \frac{|\sigma_T|\Delta T L}{\mu \kappa} \qquad (1\text{-}1),$$

$$Re \equiv \frac{Ma}{Pr} \qquad (1\text{-}2),$$

σ_T is a temperature gradient of surface tension, ΔT is a temperature difference between hot and cold disks, L is a characteristic length of the fluid, μ is dynamic viscosity, α is thermal diffusivity, and Pr is Prandtl number of the fluid. In this study, a radius (a) of the liquid bridge is used as a characteristic length.

In higher Pr number fluids, it was experimentally proved that a transition from axisymmetric steady to 3D oscillatory flow occurs at a critical Marangoni number (Ma_c). On the other hand, it was numerically predicted that thermocapillary flow in a low Pr number had two transition points [1], [2]: That is, transition from axisymmetric to 3D steady will occur at a first bifurcation point (Ma_{c1}), and transition from 3D steady to oscillatory at a second one (Ma_{c2}). The prediction needs to be experimentally proved.

A detail experiment around the bifurcation point, in which even the Ma_{c2} is predicted to be in the order of 10^1 for a Pr =0.01 liquid bridge [3], is required to prove the transition behavior of Marangoni convection. However, many studies have been conducted at a Marangoni number that is far from the Ma_{c2} because those have mainly focused on a contribution to produce a high quality single crystal from a molten metal.

Nakamura et al. [4], [5] measured a surface temperature fluctuation with a thermocouple in a molten silicon column of 10mm in diameter and 10mm in length, and found that a frequency of the fluctuation was 0.1Hz at a temperature difference of 100K. However, the imposed temperature difference was far from the second bifurcation point. Han et al. [6] experimentally investigated thermocapillary convection in a liquid bridge of mercury. Free surface fluctuations were measured by a non-contacted diagnostic system, and they found the Ma_{c2}, detecting it to be 900 with a frequency around 5Hz. Quite recently, Yang and Kou [7] reported the onset point of temperature fluctuation and its frequency (Ma_{c2}=194 and 1.1Hz) of a molten tin column by the contacted diagnostic, *i.e.* J-type thermocouple. However, disturbances on the flow and temperature field are caused by a thermocouple which contacts

with a fluid and a thermocouple often acts as a cold spot which makes it a complicated temperature gradient along a free surface. It should be noted here that there is no successful experiment to verify the transition behavior of thermocapillary flow by a non-contact diagnostic even nearby the Ma_{c2}.

The goal of present study is to understand the transition phenomena of thermocapillary flow by means of an experimental approach and comparative study with the numerical works in this research group.

The experimental efforts began to select a fluid material for a low Pr number liquid bridge in 1998 [8]. The selected material was molten tin of which Pr number is identical with that of molten silicon (Pr =0.01). Therefore, we can directly compare our experimental result with available experimental and numerical results of molten silicon because the identical Pr number means to show the same fluid dynamic behavior. Moreover, molten tin as a test fluid has an experimental advantage in a detection of Ma_{c2} compared to molten silicon. Since the melting point of tin is much lower than that of silicon, there is no need to use an infrared image furnace for melting a tin sample, which was used for a molten silicon experiment [4] and [5], and an electric heater is applicable to melt it. Thus, it is expected that the surface temperature of a molten tin column can be measured by a non-contact diagnostic with relatively low noise level. The high purity iron was selected as solid material to sustain a liquid bridge because of the reason that moderate wettability and low reactivity against molten tin is required for the solid material [8].

On the other hand, the selected test fluid has a thermodynamic disadvantage which the oxygen partial pressure is extremely low at the equilibrium between molten tin and tin oxides (SnO and SnO_2) near the temperatures for the low Pr experiment (about 570-770K), resulting in suppressing the thermocapillary flow by the formation of an oxide film over a surface of the melt. However, in 1999, we have successfully overcome the difficult problem of oxidation over the tin surface [9]. Consideration concerning the surface science of tin led us to design of a unique experiment apparatus where a clean surface of molten tin can be obtained by the Ar^+ ion etching method and sustained under the high vacuum condition (about 10^{-6} Pa) during an experiment. The performances of the experiment apparatus were already confirmed. In 1999, a non-contact measurement technique of the surface temperature has been also developed to detect small amplitude of temperature fluctuation at around the Ma_{c2} [9]. It was also confirmed that the radiation thermometer which is equipped with the PbS photo detector and combined with the attachments to obtain a high signal-to-noise ratio such as CaF_2 optical pass filter and an isotropic graphite panel had the sufficient temperature resolution to detect the Ma_{c2} with high accuracy. It was concluded that those unique considerations and devices undoubtedly lead us to a success of detecting the transition to oscillatory flow of the low Pr fluid without any flow disturbances.

Compared with the conventional transparent fluid used for a high Pr number experiment, a low Pr number fluid has another experimental difficulty: It is impossible to observe an internal flow field for opaqueness of a low Pr fluid. In order to overcome this problem, a novel visualization technique using an ultrasonic transducer with a high heat resistance has been experimentally studied for an internal flow field measurement since 1999 [9]. The visualization technique also requires a development of a unique balloon-like tracer. A critical condition on the Ma_{c1} and a detail structure of oscillatory flow will be clarified by this measurement technique.

The experimental results with molten tin obtained in 2000 are significant for the thermocapillary convection of a low Pr fluid. As predicted in the last issue [9], we have succeeded in detection of the transition to oscillatory flow by the surface temperature

measurement without any flow disturbances. The flow transition was verified by comparison of the experimentally obtained Ma_{c2} and frequency of surface temperature fluctuation with the numerical results, and by a surface flow visualization experiment directly [10]. The effect of the liquid bridge geometry on the Ma_{c2} and oscillation frequency was further investigated and discussed [11]. The following results are described in this study:

(1) Experimental verification of surface temperature measurement (in-house activity)
(2) Detection of transition phenomena to oscillatory flow (in-house activity)
(3) Effect of aspect ratio on the critical condition and flow structure (in-house activity)
(4) Numerical simulation for the specific case (collaboration with Kyushu University)
(5) *in-situ* measurment of surface tension of the molten tin
(6) Development of measuring technique of internal flow field (entrusted to Toshiba Co.)
(7) Development of visualization tracer (collaboration with Kagoshima Prefectural Institute of Industrial Technology and partly entrusted to NTT Advanced Technology Co.)

2. OSCILLATORY THERMOCAPILLARY FLOW OF MOLTEN TIN

2. 1 Experimental Setup

The experimental apparatus is shown in Figs 2-1, 2-2, 2-3 [8,9,10]. It consists of a liquid bridge formation part, a measurement region, a sample supplying system and a sample cleaner. The liquid bridge was formed by sandwiching between a pair of pure iron disk (purity: 99.5%). All experiments were done in the ultra high vacuum conditions, which were under 10^{-5}Pa, to keep clean sample surface and less heat loss of molten tin liquid bridge. To impose the temperature difference, the lower disk was cooled by helium gas and the upper disk was heated by an electric resistant heater. The electric heaters were not controlled by PID (Proportional, Integral and Derivative) control to circumvent the temperature hunting phenomena. The temperature difference was gradually increased from around 0K to above the onset. An imposed ΔT was measured with the thermocouples embedded at near the end face of the disks.

Solid tin (purity: 99.999%) is melted in a quartz tube as illustrated in Fig. 2-2. The melt is supplied onto the lower disk *via* the capillary portion (1mm in inner diameter) of the quartz tube where bulk oxide in the crude fluid can be removed. For further purification, Ar^+ ion etching method was applied and the ion gun designed for surface cleaning was installed in the chamber. Surface temperature of the liquid bridge was measured with a radiation thermometer, in which PbS photo detector was installed, mounted on outside of the chamber.

The lower disk was optimized to measure the temperature field of liquid bridge as shown in Fig.2-3. The measurement of temperature field was necessary to understand the oscillatory thermocapillary convection. Because of the motion of temperature field was coincided with the one of oscillatory flow. It has been inserted some ϕ0.3 mm K-type thermocouples (TC) sheathed a stainless steel in these 0.35 mm-holes. The top of thermocouples was adjusted the same position as lower disk plane.

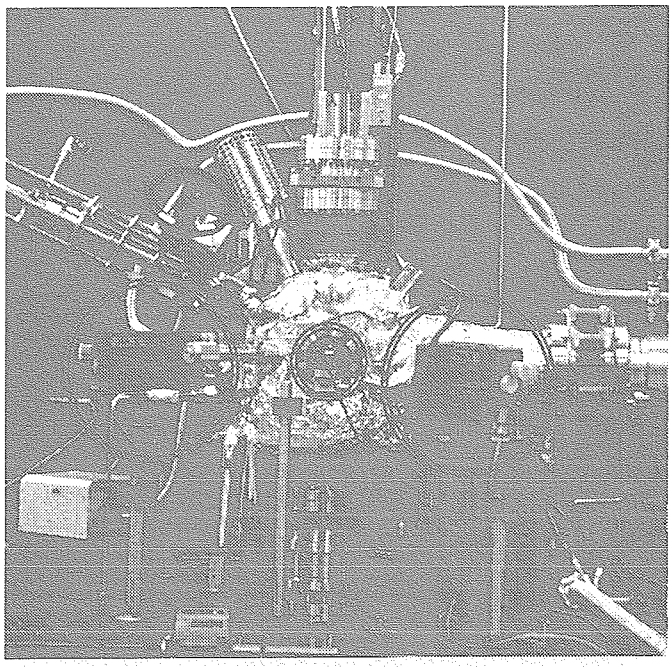

Fig. 2-1 Experimental equipment

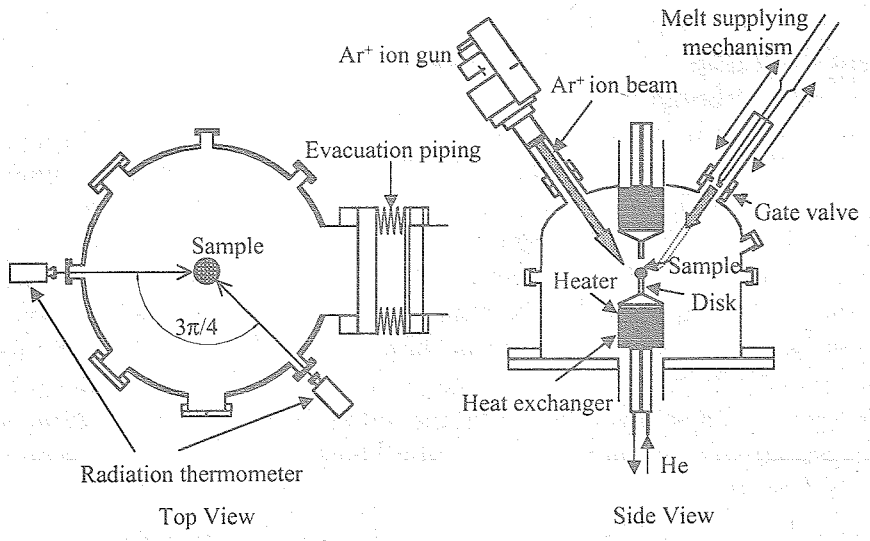

Fig. 2-2 Schematic diagram of experimental equipment

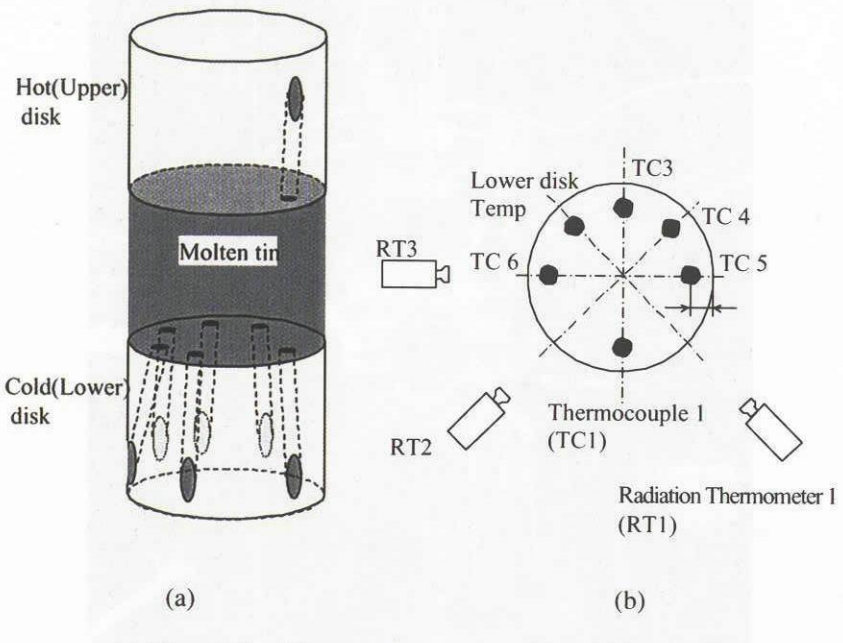

Fig. 2-3 Temperature measurement points
(a) Schematic diagram of tin liquid bridge and disks
(b) Lower disk surface and positions of radiation thermometers

2.2 Improvement of Experimental Techniques

(1) Purification of liquid bridge

The purity of formed liquid bridge is very important because an oxide on a free surface can change the surface tension. Therefore the purification of supplied molten tin should be done. As mentioned above, the experimental equipment already has a sample cleaner system, such as Ar^+ ion gun, high vacuum chamber, and sample supplying capillary tube. In addition to these, a stainless steel mesh filter was installed in the capillary tube. It can stain off the crude fluid, which is mainly oxide, from supplying molten tin. The capillary tube for sample supplying system is shown in Fig.2-4. Molten tin flows from left fat to right thin parts. In the case of no filter, a white powder-like sludge adhered on the inwall of slim part of capillary tube. On the other hand, the mesh filter worked very efficiently, because no sludge can be found below the filter in Fig. 2-4. Consequently, the liquid bridge could be refined.

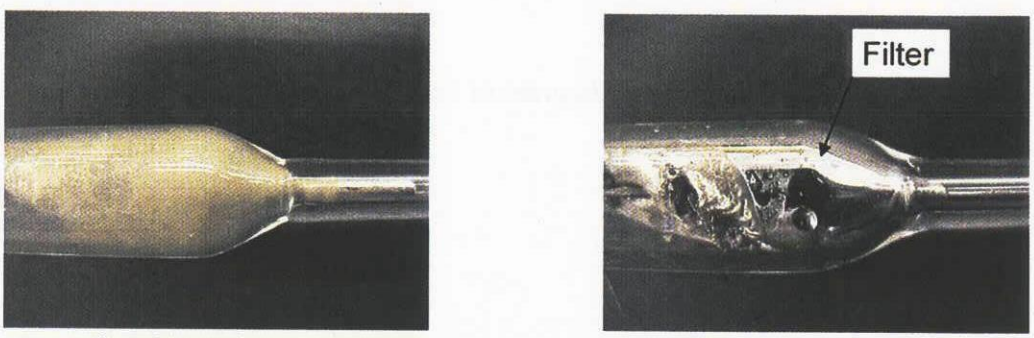

(i) without filter (ii) with 0.1 mm mesh filter

Fig. 2-4 Improvement of sample supplying tube

2.3 Detection of Onset of Temperature fluctuation

As described in previous annual report, we succeed to observe the onset of the oscillatory thermocapillary convection in low Prandtl number fluid. And it was also mentioned that a number of data, which were measured by radiation thermometers, enable us to classify the patterns of surface temperature fluctuation (STF) at the transition into 5 types as follows;

1: Start STF with low* frequency -> Stop STF ->Restart STF with high* frequency
2: Occurrence of temperature shift (one-time) -> No STF -> Start STF with High frequency
3: Start STF with low frequency -> Frequency of STF become higher
4: Start STF with low frequency. After that, frequency of STF becomes higher with increasing ΔT.
5: Start STF with high frequency
* Definition of frequency speed (order of magnitude); Low: 10^{-2}Hz, High: 10^{-1}Hz

So, we tried to make clear the transition phenomena in detail. In addition to radiation thermometers for temperature measurement, the thermocouples inserted in the cold disk were used. The temperature measurement point is shown in Fig. 2-5. The three radiation thermometers and four thermocouples were employed.

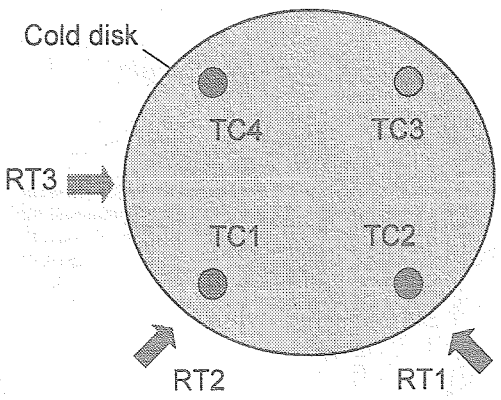

Fig. 2-5 Position of radiation thermometers and thermocouples (top view)

The type-1 transition of temperature fluctuation was frequently observed. Figure 2-6 shows time variation of temperature at the first onset, which Marangoni number was 124 and aspect ratio 1.2. After the onset, oscillatory temperature variations could be observed as shown in Fig. 2-7. The phase relations against TC2 are also illustrated in this figure. RT1 and TC4 were in phase with TC2, but TC3 was out of phase with referenced TC2. So, this oscillation mode could be assumed mode 2 and rotation type (2R mode). The oscillation with low frequency around 0.02 Hz continued until Ma = 132 and it stopped at higher Marangoni number. When the temperature difference ΔT increased furthermore, the oscillation occurred again but with medium frequency about 0.3 Hz, which is shown in Fig. 2-8.

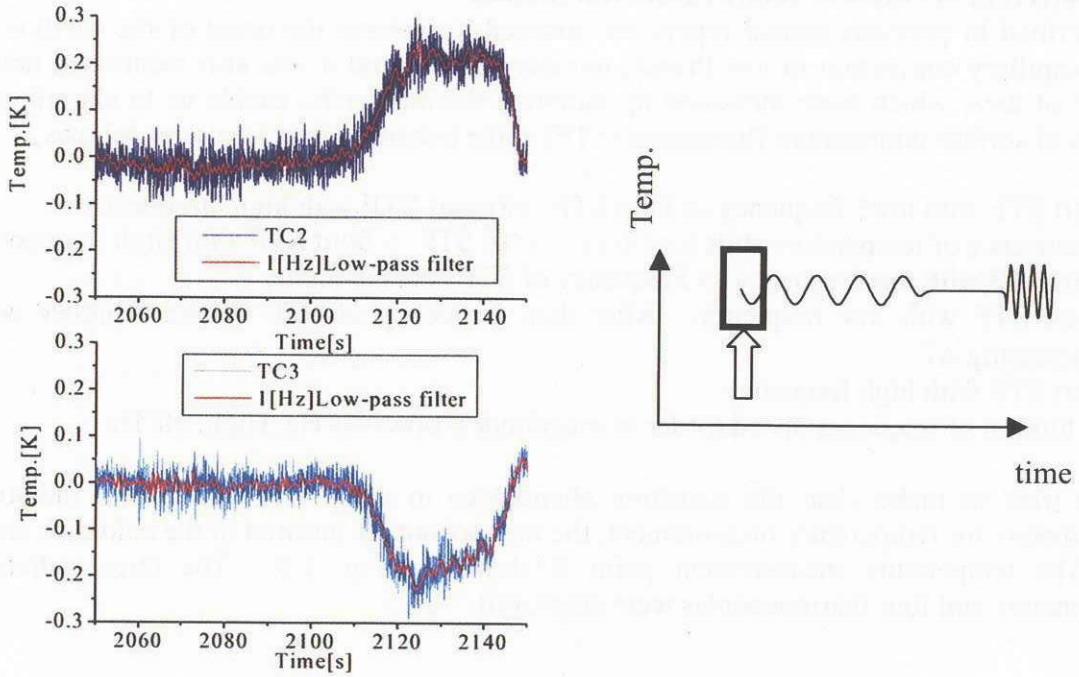

Fig. 2-6 Onset of low frequency oscilation

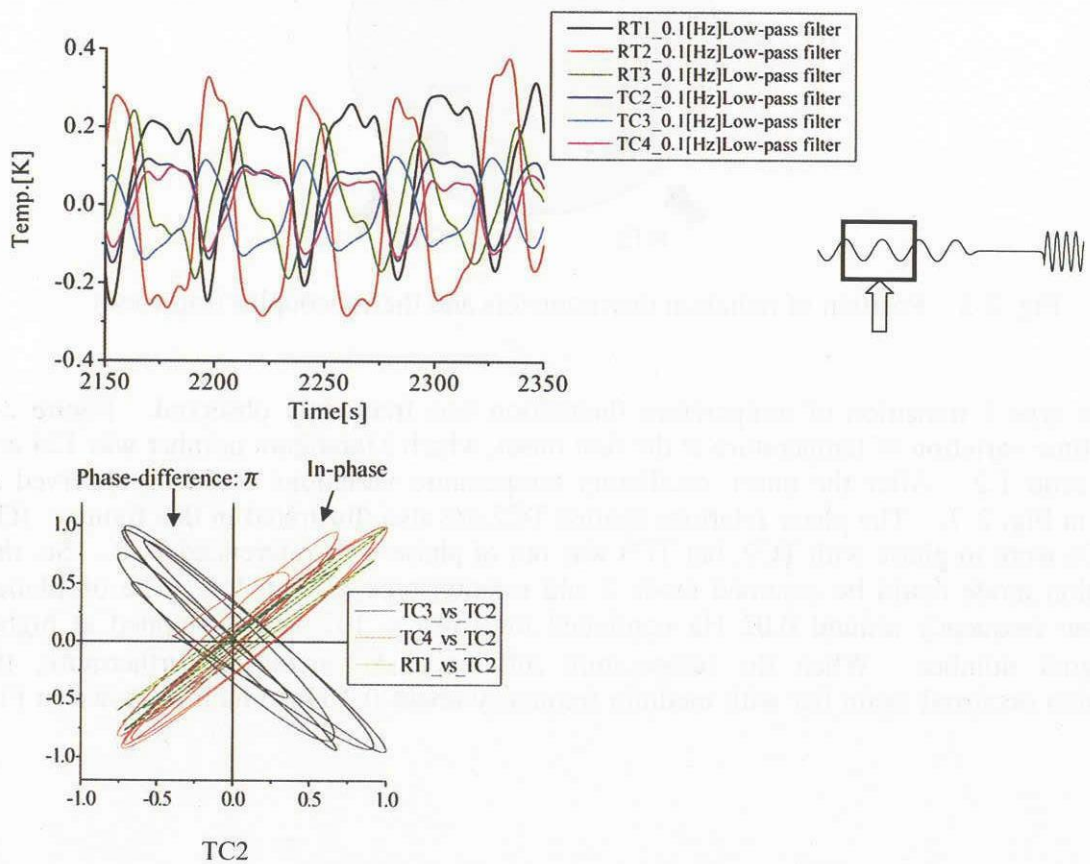

Fig. 2-7 Time variation of temperature and cross-correlation between TC3, TC4, RT1 and TC2

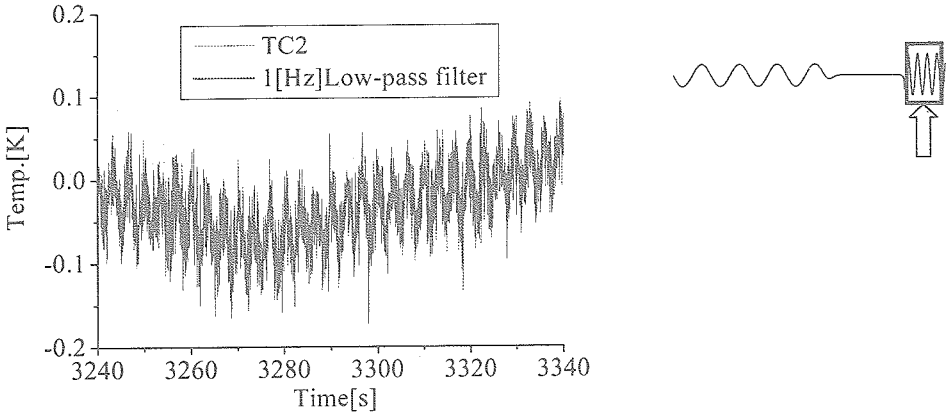

Fig. 2-8 Onset of medium frequency oscillation

A numerical simulation done by Prof. Imaishi *et al.* makes us understood the above transition process. In this simulation, the time history of temperature difference corresponding to our experiment was used. Figure 2-9 shows the time variation of surface velocity and temperature. It is clearly seen that the first transition (Ma_{c1}) at around t = 55 s and the second transition (Ma_{c2}) with high frequency at around t = 220 s were occurred. The most notable point is that the low frequency oscillation with large amplitude at t = 250 s appeared after starting the oscillation. After that, the oscillation shifted medium frequency at around t = 350 s. Those behaviors seem to be similar to the experimental results except for high frequency stage. Experimentally, the low frequency oscillation could be sensed at first because the amplitude of temperature oscillation became detectable. So, we need to observe a flow field to detect the first transition (Ma_{c1}) and the second transition precisely.

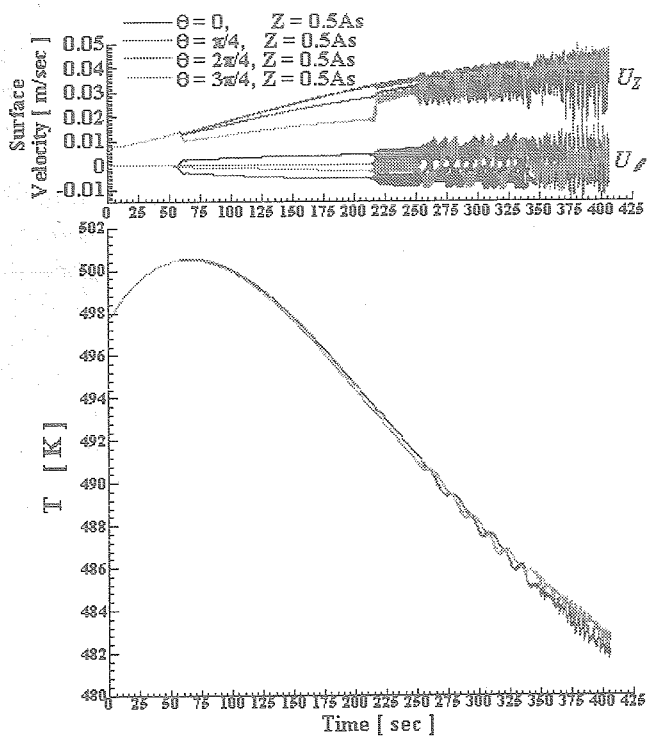

Fig. 2-9 Transition process by numerical simulation (Imaishi *et al.*)

2.3 Effects of aspect ratio

(1) Experimental conditions

The disk diameters from 3.0mm to 7.0mm were used in order to covering liquid column with aspect ratio (*As*: height/radius) from 0.8 up to 2.2. This range almost corresponds to calculated range of numerical simulation by Imaishi *et al.* [13]. Heights of the liquid column were adjusted in from 1.5 mm to 4.5 mm at all the experimental cases, minimizing the dynamic bond number *Bd* (*Bd*<1).

$$Bd \equiv \frac{\rho g \beta L^2}{\sigma_T} = \frac{Ra}{Ma}$$

where ρ, is density, g gravitational acceleration, β volumetric expansion coefficient, σ_T temperature gradient of surface tension, L the height of the liquid column and Ra is Rayleigh number. However the static bond number B_0 is larger than unity, volume ratio or diameter ratio (D/D_{max}), surface shape is almost straight.

$$B_0 = \frac{\rho g L^2}{\sigma}$$

In every case, temperature difference (ΔT) was imposed at certain changing rate. In some cases, ΔT was reduced after transition in order to measure surface temperature behavior when damping. Since the control of changing rate of ΔT (dΔT/dt) is very difficult, there were some widths on them. Influence of ramping rate of temperature difference, dΔT/dt on transition was discussed in previous report. The dΔT/dt ranging from 0.4 to 2.1 K/min has no influence in the critical Marangoni number. Therefore we controlled the dΔT/dt around 0.5 K/min.

(2) Ma_c as a function of aspect ratio

In order to make clear the influence of aspect ratio on Ma_{c2}, the onset of oscillatory thermocapillary flow using liquid columns with As from about 0.8 to 2.2 are investigated. In the case of experimental work in this case, Ma_{c2} is determined by the temperature difference at the onset of low frequency oscillation. It seems reasonable because the Ma_{c2} at the second transition point was slightly 10 % higher than the first point.

The Ma_{c2} as a function of *As*, which was experimentally and numerically obtained by Imaishi *et al.* [13], are shown in Fig. 2-10. The estimated oscillation mode is also described in this figure. The experimental Ma_{c2} in the range of *As* higher than about 1.2 well corresponds to numerical one. The experimental Ma_{c2} increases with decreasing of *As* monotonically. In contrast, the numerical Ma_{c2} has a peak at $As = 1.2$ and the one slightly decreases when As in the range of $1.0 \leq As \leq 1.2$ decreases. The experimental results showed that the Ma_{c2} ($As \leq 1.3$), which was obtained using the liquid column with relative large radius and the one lied on relative low Marangoni number, was obtained by the experimental conditions at small dΔT/dt. We will make clear the reason why the experimental critical Marangoni number in the smaller aspect region differs from the numerical result in near future.

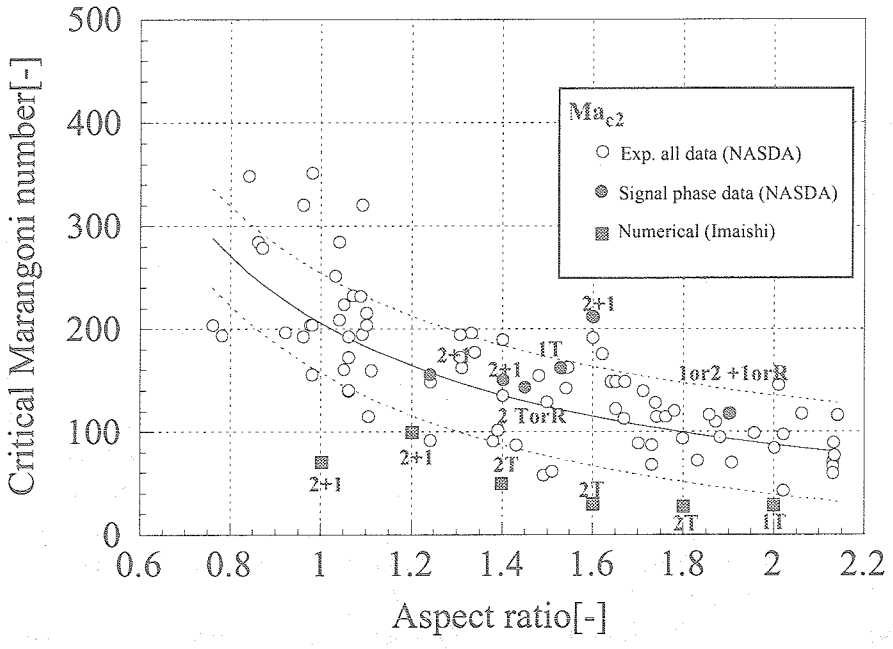

Fig.2-10 Dependence of Marangoni number on aspect ratio

3. *IN-SITU* MEASUREMENT OF TEMPERATURE COEFFICIENT OF SURFACE TENSION OF THE MOLTEN TIN

3.1 Introduction

The surface tension and its temperature coefficient are very important factors to understand the thermocapillary convection and it is well known that the surface tension was strongly affected by the oxygen. Yuan *et al.* [14] presented the temperature coefficient of surface tension of molten tin at normal pressures of Ar gas, which was controlled the oxygen partial pressures (P_{O2}). Passerone *et al.* [15] presented the surface tension and its temperature coefficients of molten tin at the helium + 5% hydrogen gas of normal pressures, the helium gas of normal pressures and the vacuum conditions (5×10^{-4} to 1×10^{-5} [Pa]). The temperature coefficients were different on each condition. The surface tension is affected by the atmosphere, especially the gas flux and P_{O2}. However, the vacuum condition was not discussed well. R.Sangiorgi *et al.* [16] presented the relationship between the molten tin surface tension and the intensities of auger spectrum at 560[K]. In the case of the ratio of intensities(R), which were the auger spectrum intensity of oxygen and tin, was less than 0.2, the surface tension was about 600[mN/m]. However, R was more than 0.2, the surface tension was decreased to about 535[mN/m] at 5×10^{-2}[Pa].

Nevertheless, the thermocapillary convection experiments have been done at the ultra high vacuum (UHV) conditions, which total pressures were under 10^{-6}[Pa], the P_{O2} and R-value were not clarified. Because of it is very difficult to measure the P_{O2} in such UHV conditions. The surface tension and its temperature coefficient should be measured in the experimental chamber.

3.2 Surface tension measurement procedure

A molten tin droplet, which was supplied through a quartz capillary tube to remove oxides in the liquid state, was formed on an α-Al_2O_3 substrate in the evacuated experimental chamber. The substrate had been heated at the experimental temperature. The shapes of droplet were taken by a camera. Photo-images were taken between 550[K] and 773[K] with the increasing temperature and the decreasing temperature. These analog photo images were transfer to digital images and the surface tension was calculated from the outlines of digital image, which was the sessile drop method.

3.3 Results

There was not any effect of the temperature coefficient of surface tension between the increasing and the decreasing temperature conditions. Figure 3-1 shows the results of surface tension measurement in this work, Yuan *et al.*, Passerone *et al.* and Sangiorgi *et al.*. The value of surface tension and its temperature coefficient were 520~550 [mN/m] and 0.097 [mN/m/K] in this work. The value of surface tension was agreed well with the results of Passerone *et al.* [15] reported that the values of surface tension were scattered from 500 to 600 [mN/m] near the melting point on high P_{O2} conditions. In this study, these values were not scattered in this temperature region compared with their results. Therefore, the P_{O2} in this chamber was very low and prevented the oxidation of molten tin surface. The value of its temperature coefficient was similar to the one of $P_{O2}=10^{-15}$ [MPa] in the results of Mukai *et al.*.

This droplet was held for long time. Therefore, these results were measured near the equilibrium conditions. However, the molten tin surface was refined by a quartz tube before the thermocapillary convection experiment, the molten tin surface was not equilibrium conditions. R.Sangiorgi [16] reported as-melted surface tension of molten tin was changed

after holding for 57.6[ks] at 4×10^{-5} [Pa]. Therefore, it was a possibility that the surface could react to the residual oxygen in the chamber and then the surface tension was changed during the thermocapillary experiment. We should investigate the time dependency of surface tension.

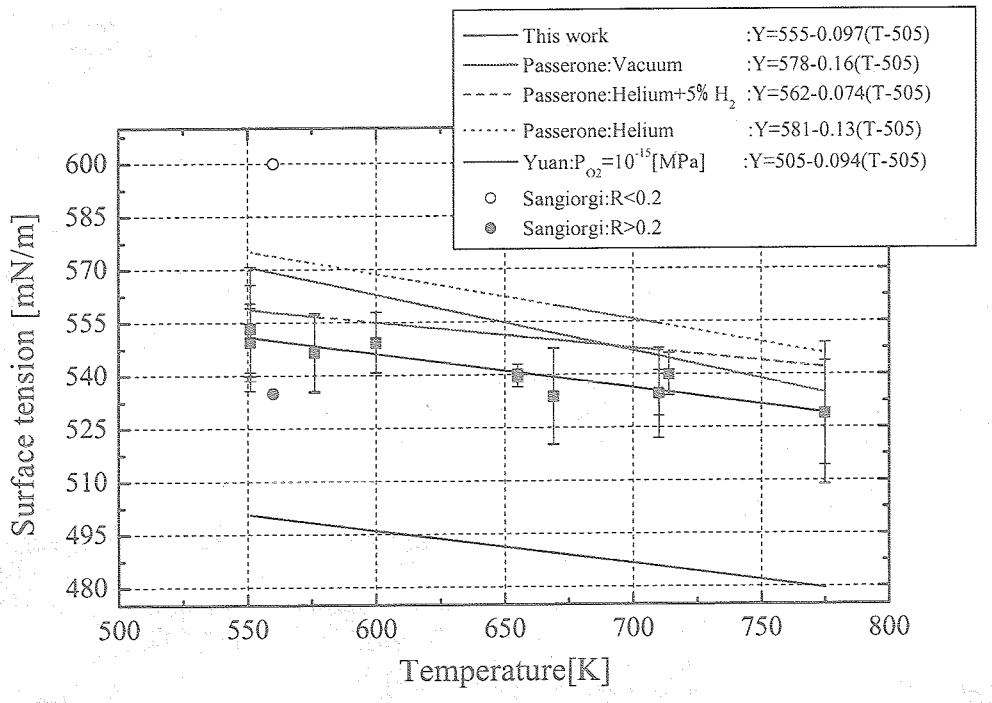

Fig.3-1 Surface tension of molten tin against temperature at 10^{-6} [Pa]

4. DEVELOPMENT OF TRACER PARTICLE FOR 3D-UV

4.1 Selection of Shirasu-balloon

The observation of inner flow pattern of the Marangoni convection by means of above-mentioned 3D-UV technique is mainly done under extreme conditions, which are high temperature and low pressure conditions. The tracer particles, hence, should be manufactured so as to endure such condition. Furthermore, for obtaining high signal from a tracer particle, the particles are required to have high reflectance of ultrasonic beam (US beam). Since the target value of the reflectance is up to 95 % when above-mentioned 3D-UV technique was used, acoustic impedance of a tracer particle should be less than 0.4×10^6 kg/m^2/s. Considering this acoustic impedance, it is only attainable to make a "balloonlike structured tracer particle" because acoustic velocity is extremely high, which is approximately 2,570 m/s in molten tin and balloons are not able to suspend in the molten tin under normal gravity. Now, we propose a very unique feature of the balloon tracer that can be actually manufactured. Table 4-1 tabulates the qualitative evaluation of balloons and several porous materials. Selection of Shirasu-balloon (SB), which is an expanded volcanic particle, as the base material for the tracer particle is reasonable because the SB shows high thermal stability and is available size with our target diameter.

Table 4-1 Qualitative evaluation of balloons and porous materials

	Sphericity	Available size [μm]	Capability to maintain its void in melt	Heat resistance at 773K	Total evaluation
porous SiO_2	○	1-150 ×	×	○	×
porous glass	○	100-500 ○	?	△	×
Shirasu-balloon	△	10-1000 ○	○	○	○
pearlite	×	>150 ○	×	○	×
glass balloon	○	10-100 △	○	△	△
Al_2O_3 bubble	×	?	?	○	×
TiO_2 balloon	○	30-50 ×	?	○	×

Shirasu: glassy volcanic fragment distributed in southern Kyushu, also named Hakudo

4.2 Conditions as a tracer particle

The SB particles should have following characteristics as tracer particles: high thermal stability, high wettability and low reactivity with surrounding molten tin. With regard to the shape as a tracer particle, high sphericity is also required. The high wettability and low reactivity strongly requires a thin metal coating layer on the SB particle. Therefore, multi-layer structure was adopted. Figure 4-5 shows the schematic of the multi-layer structure and selected metals of the SB particle. The inner layer plays a role of keeping high sphericity. The SB particle is a kind of expanded particles so that its feature was not sphere, and the surface was also rough. Coating the nickel (Ni) layer will improve sphericity of the SB particle with smooth surface. The outer layer works as a reaction layer with surrounding fluid. The iron (Fe) layer reacts with molten tin in moderation, and keeps wettability with surround on surface. The thickness of the layer plays a role of adjusting a density of the SB particle with molten tin.

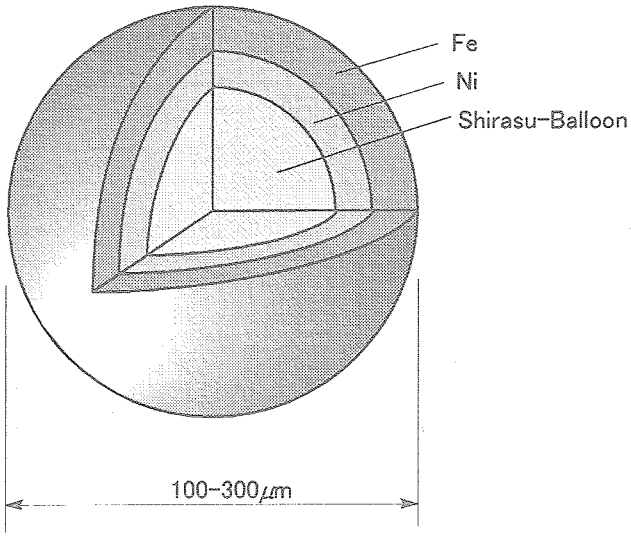

Fig.4-5 The multi-layer structure and selected metals

4.3 Consideration Point

Since density of the tracer particle has to be close to that of surrounding fluid, molten tin (approx. 6.7×10^3 kg/m^3 at 673 K) for a ground-based experiments, thickness of Fe layer should be estimated precisely. The thickness of Ni layer is fixed to 40 μm from the view point of manufacturing technique. The SB particle covered with 40 μm Ni layer (Ni/SB) is lighter than the molten tin, so that the heavier metal should be plated on the surface so as to adjust the density of the tracer particles with surrounding molten tin. **Figure 4-6** shows the relationship between specific gravity (ρ_{tracer} / $\rho_{surround}$) and Fe layer thickness. When the Ni/SB particle is small (*i.e.* 100-150 μm in diameter), the thickness of Fe plating layer is enough to be only 30-40 μm. However, the large one requires over 100 μm thickness of Fe plating layer. It of course occurs technical issues.

In general, thickness of a film that can be grown by sputtering is only a few microns. Therefore, surface modification of the SB particle should be carried out by not sputtering but plating of Fe. Since the SB shows excellent electric insulation and electroless Fe plating is impossible, the plating should be conducted as following processes:

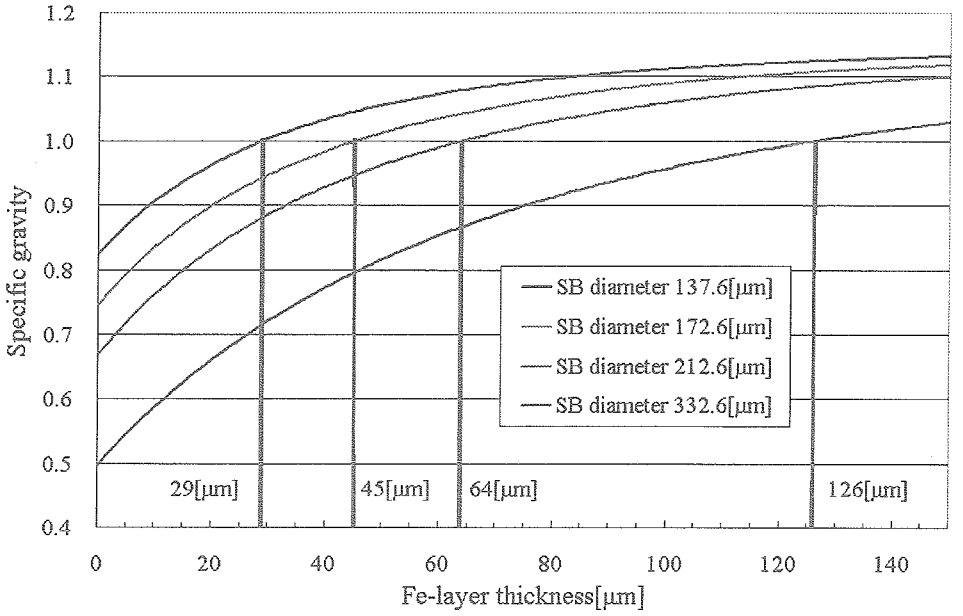

Fig.4-6 Relationship between specific gravity and Fe layer thickness for various diameters of the SB particles

1st stage: Electroless Ni plating

$$Ni^{2+} + H_2PO_2^- + 3OH^- \rightarrow Ni + HPO_3^{2-} + 2H_2O \quad (4\text{-}1)$$

2nd stage: Electrolysis Fe plating

$$Fe^{2+} + 2e^- \rightarrow Fe \quad (4\text{-}2)$$

At the viewpoint of traceability of the particles, the maximum diameter of tracer particle must be less than 670 μm in the case that the molten tin was test fluid. On the other hand, the 3D-UV system requires that the particle diameter is over 300 μm in order to detect the signal echo from the particle. Finally, by simple estimation, the overall features of the tracer particle (approx. 300-600 μm in diameter) will be as follows: diameter of the SB is 150-300 μm and thickness of plating layer of Ni and Fe are 40 μm and 35-110 μm, respectively.

4.4 Plating Technique

Elemental techniques that should be developed are a method to improve sphericity of the SB and a plating condition to obtain smooth surface of Ni and Fe. We firstly studied the development of the plating technique. Since using a small SB particle (*i.e.* 90-100 μm in diameter) makes it difficult to handle the particles during the plating and to analyze a plating layer, 1000 μm-class SB, which was produced as an expanded perlite by Fuyolite Co. Ltd. and named "Fuyolite #1", was adopted for the development phase. However, since the sphericity of Fuyolite #1 was not good; it can be easily considered that the uniform thickness of the plating layer has affected the shape of the tracer particle. The cross-sectional observations by Optical Microscope (OM) and Scanning Electron Microscope (SEM) have enabled us to resolve this consideration. The result was that the sphericity of 100 μm-class SB particle has improved by preliminary experiments.

4.5 Ni coating

The trial experiment was conducted for development of electroless Ni plating technique over the 1000 μm-class SB particle as shown in **Fig. 4-7** (named "Ni/SB #1" hereafter). In this experiment, a plating solution ($NiSO_4$ aqueous solution) and a reducing agent for Ni^{2+} (NaH_2PO_2) were simultaneously added to the SB particle which was dispersed mechanically in water, in which molar ratio of $H_2PO_2^-$: Ni^{2+} was kept constant at 3:1. **Equation 4-1** is an equimolar reaction; hence, the excess degree of $H_2PO_2^-$ in a reaction vessel will become larger in the case of the plating, resulting in accumulation of non-reacted $H_2PO_2^-$ in the plating layer by physical absorption. The SEM images clearly showed that the columnar crystal growth occurred whole period of the reaction. The elemental analysis of the plating layer by Auger Electron Spectroscopy (AES) revealed that nickel oxide(s) of 5 nm in thickness existed on the surface and high concentration of Ni in the bulk. Electrolysis Fe plating was carried out over Ni/SB #1 sample by using $FeSO_4$, H_2SO_4, and H_3BO_3 electrolytes and a basket-type galvanic cell.

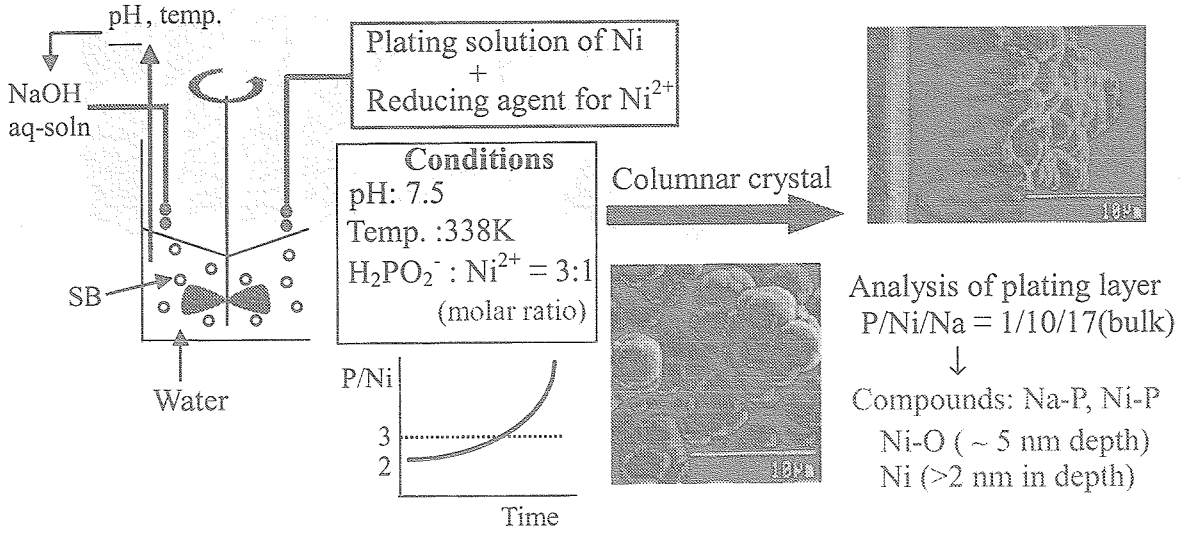

Fig.4-7 Trial experiment of electroless Ni plating over 1000 μm –class SB plating solutions and reducing agent were simultaneously added.

It is well known that the columnar crystal growth often occurs under high concentration of $H_2PO_2^-$ and passivity of Ni-oxide film increases with content of $H_2PO_2^-$. Therefore, the feeding method of the plating and reducing agent of Ni^{2+} should be improved under the condition of reducing concentration of $H_2PO_2^-$. However, secondary surface oxidization of the Ni/SB is unavoidable because Ni is a base metal and the surface of the Ni/SB particle is quite important for the next process, the Fe plating. And high conductivity is required for electrolysis plating; thus, corrosive material should be increased by addition of hydrochloric acid (HCl) to the electrolyte of Fe plating.

Figure 4-8 shows the improved method for the Ni plating. The 1000 μm-class SB was dispersed in $NiSO_4$ aqueous solution (0.095mol/l) and only the reducing agent (NaH_2PO_2) were added to the reaction vessel with keeping constant pH of 6.0 (named "Ni/SB #2",

hereafter). The overall molar ratio of $H_2PO_2^-$: Ni^{2+} was also 3:1, however, it was easily inferred that the real ratio in the vessel approached to zero in the initial period of the plating with the dropping method. The SEM images showed that the Ni layer proceeded almost whole period of the reaction, and the thickness of the plating layer was about 10-20 μm. The columnar crystal growth was observed only on the surface of the Ni/SB #2. This was attributable to high concentration of $H_2PO_2^-$ in the final period of the plating; thus, no columnar crystal growth will be able to be attained by further improvement of the plating technique, such as the optimization of the feeding conditions. The AES analysis of the plating layer revealed that the thickness of Ni-oxide(s) film decreased from 5.0 nm to 1.6 nm and metallic Ni also existed on the surface.

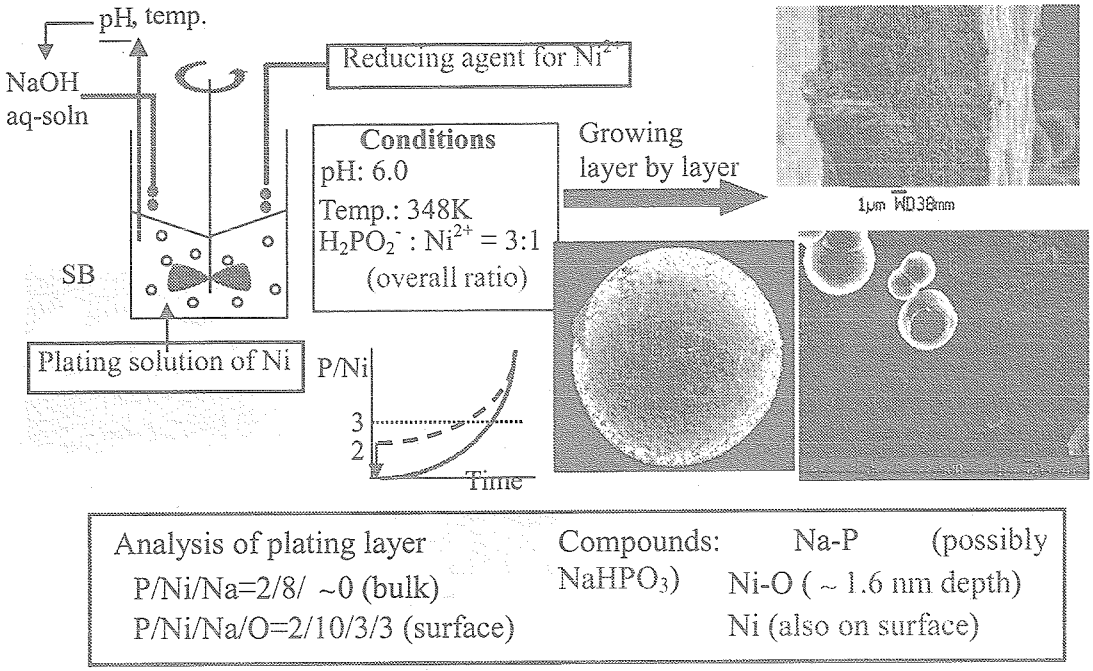

Fig.4-8 Improved method for electroless Ni plating only reducing agent was added.

4.6 Fe coating

The improved method for the Fe plating is shown in **Fig.4-9**. For increasing corrosive material, a mixed electrolyte of $FeSO_4$ and $FeCl_2$ (9:1 in molar ratio) was used in mixed acidic medium of HCl and H_3BO_3 (pH < 2.0). Moreover, a number of the brass balls (2 mm in diameter) were inserted to the basket-type galvanic cell, in which the ratio of the brass balls to the Ni/SB #2particles was about 5:1 in order to improve the contact efficiency of Ni/SB #2 with the electrode. As a result, the electrolysis Fe plating successfully proceeded over Ni surface in the cell rotating at 10 rpm for 20-30 min (named "Fe-Ni/SB #1", hereafter). The SEM images showed that smooth surface of Fe could be obtained over Ni/SB #2 particle, whereas the hill-like columnar crystal growth occurred on the surface of Ni/SB #2. However, a particle having some pores on the surface was also observed. The AES analysis of the plating layer revealed that the thickness of oxidized surface, which existed as FeO, was approximately 0.2 μm and metallic iron shell was obtained with high purity (>99%), which was 10-20 μm in thickness in the bulk as seen in **Figs.4-9** and **4-10**. Although the non-uniformity of thickness and surface morphology of Fe plating layer were observed, the

uniform plating will be attained by improvement of the feeding conditions for the electroless plating and further development of the electrolysis conditions in which the electrolysis rate can be controlled.

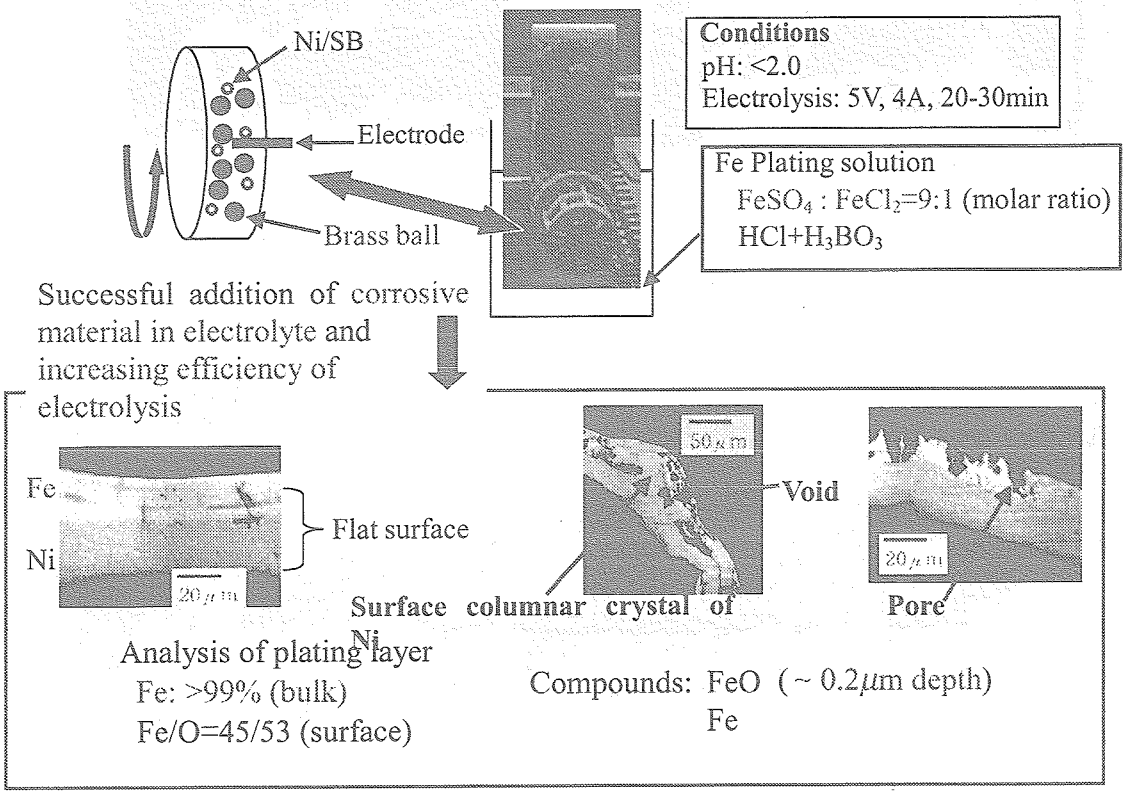

Fig.4-9 Experimental apparatus, conditions, and results of electrolysis Fe plating over the Ni/SB

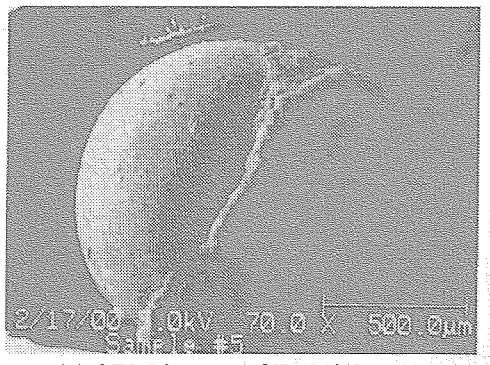

(a) SEM image of Fe-Ni/SB #1

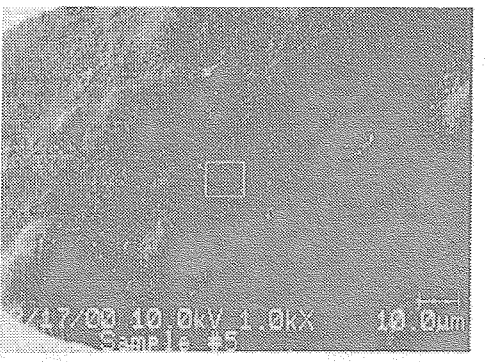

(b) Sputtering position for AES analysis

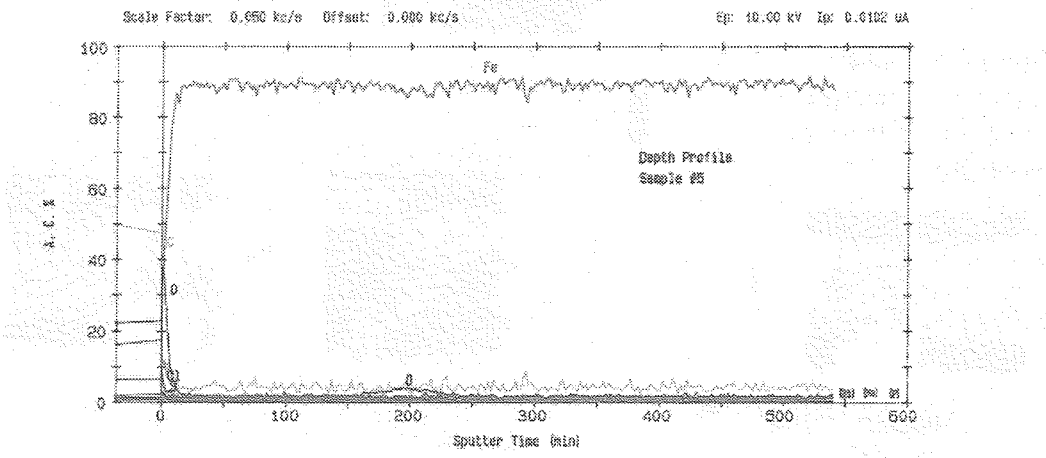

(c) Depth profile of elements in the Fe plating layer

Fig.4-10 The AES analysis of the Fe-Ni/SB #1

The Fe plating rate was also investigated in order to estimate the plating time to get the hopeful tracer particle with appropriate Fe thickness. The time variation of plating thickness is shown in Fig. 4-11. It was found that the thickness increased with the elapsed time linearly and the plating rate in case of smaller particle was slower than larger one. It can be considered that the particle size is a dominant parameter for the Fe plating rate. However, the important thing is that it also strongly relies on the conditions of plating solution. Figure 4-12 shows the Fe plating duration for various diameters of the Ni/SB particles. In this figure, the plating rate under the condition of large diameter as shown in Fig.4-11 (slower one) was adopted as a characteristic rate. A very long duration of the Fe plating for manufacturing the tracer particle, of which density is equal to that of surrounding molten tin, are required. However, it is attainable to realize the manufacture by a periodical feeding works of the plating solution.

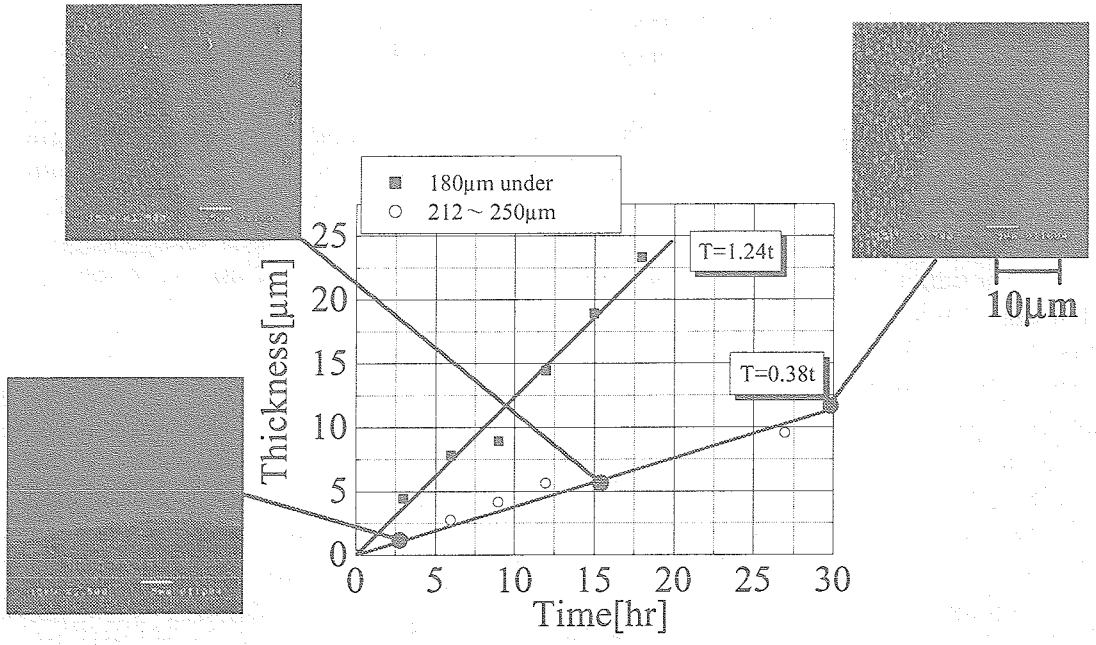

Fig.4-11 Time variation of Fe layer thickness

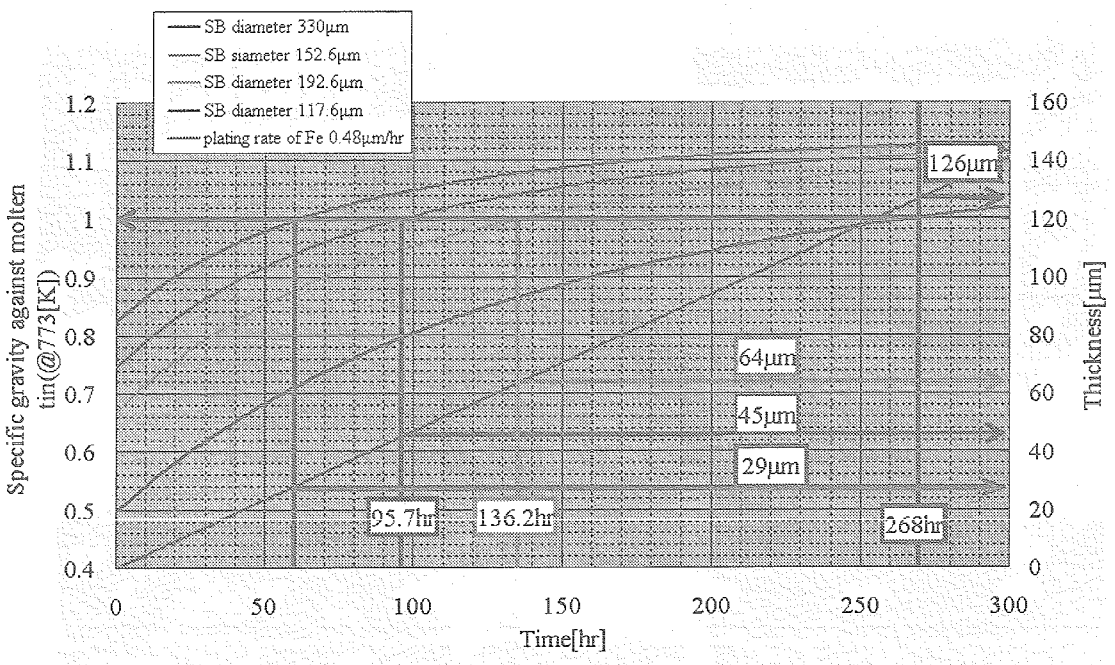

Fig.4-12 Fe plating durations for various diameters of the Ni/SB particles

4.7 Sphericity and Surface Roughness

The conventional reforming conditions for manufacturing the first-product Ni/SB particle, of which sphericity is not good, are as follows: temperature range is 1250-1350 K, a heat treatment time is approximately 0.025 sec., and an apparatus is a sand-medium fluidized bed furnace. A trial production of the Ni/SB particle was carried out under the condition of 1520 K, 0.3 sec. treatment time in an electric furnace. The result was that the sphericity of the SB particle was improved significantly. Therefore, improvement of its sphericity will be able to attain under such mild foaming conditions. From above results, we finally confirm that the balloonlike tracer particle that has good sphericity can be actually manufactured by the electroless Ni plating, subsequently by the electrolysis Fe plating.

The sphericity was improved by the above-mentioned heat treatment technique on Ni plating process. Figure 4-13 shows the Ni/SB shape before and after the heat treatment. However the shape of the Ni/SB was not good sphericity before heat treatment, the one became good sphericity with smooth surface after heat treatment.

On the other hand, the surface roughness could be improved on Fe plating process. The Fe plating layer was formed by an electrolysis plating method. The electrodes were pure iron and carbon, and the plating solution was consisted of two additives: one is saccharin ($C_7H_5NO_3S$), which absorbs on a cathode and suppresses the growth of projections. The second one is sodium dodecyl sulfate ($CH_3(CH_2)_{10}CH_2OSO_3Na$), which is used for a remover of hydrogen gas from the surface of Fe plating layer. Figure 4-14 shows the results of improvement of surface roughness. The surface roughness of tracer particle was improved clearly by the additives.

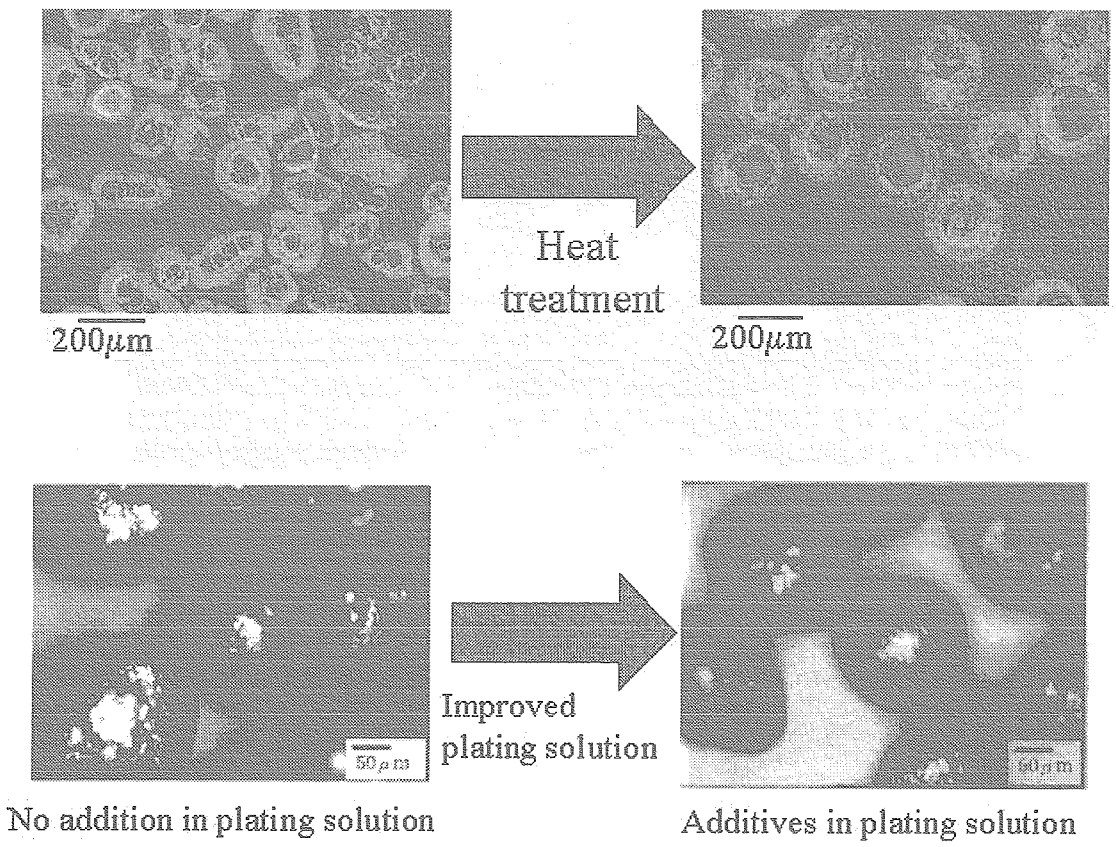

Fig.4-14 Improved surface roughness of the Ni/SB.

4.8 Environment

The Fe-Ni/SB will be exposed heat cycle during the actual thermocapillary experiment. Therefore, the following endurance test was performed. In the experiment, molten tin with some Fe-Ni/SBs was heated to 670 K and held for an hour. After that, it was cooled down to 520 K. After this sequence, it was heated again to 670 K and held for half an hour. These processes have been done in a quartz tube in which atmosphere was maintained at low vacuum condition (under 10^{-3} Pa).

It was confirmed that most of tracers were not collapsed but contained in tin melt after the experiment. The interface of Fe plating layer and tin were observed and analyzed by electron probe micro analyzer (EPMA) as shown in Fig. 4-15. The Fe plating layer became thinner than the initial thickness (20μm). Since the pure iron is oxidized very easily, the decreasing of Fe layer thickness was regarded as the result by peeling of the FeO layer. After peeling of the layer, the intermetallic compounds of $FeSn_2$ were formed on the interface.

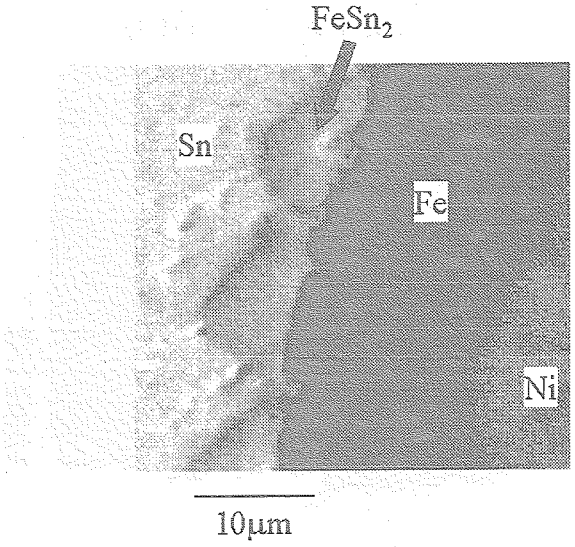

Fig.4-15 Photo of the layer interacted between Fe layer and molten tin

4.9 Check for Reflect Echo

The above-mentioned tracer particle was found in a tin bulk to check the detectability of US beam from particle. The position of particle was measured C-scan probe. Figure 4-16 shows the result of position measurement of both ϕ 1 mm and ϕ 0.1 mm particle. This image was drawn from the amplitude of echo obtained by scanning the ultrasonic beam on the tin bulk. It can be verified that the Fe-Ni/SB even in ϕ 0.1 mm reflected the ultrasonic beam. The depth of ϕ 1 mm particle was 5 mm from the top and that of ϕ 0.1 mm particle was 6 mm. We will use the tin bulk with a particle to check the sensitivity of matrix sensors.

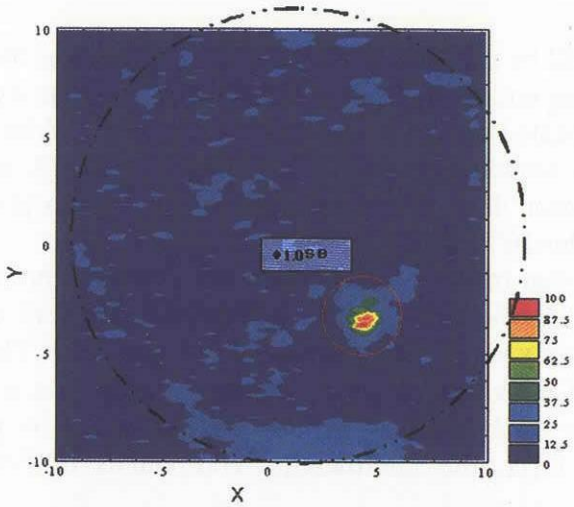

(a) ϕ 1 mm particle

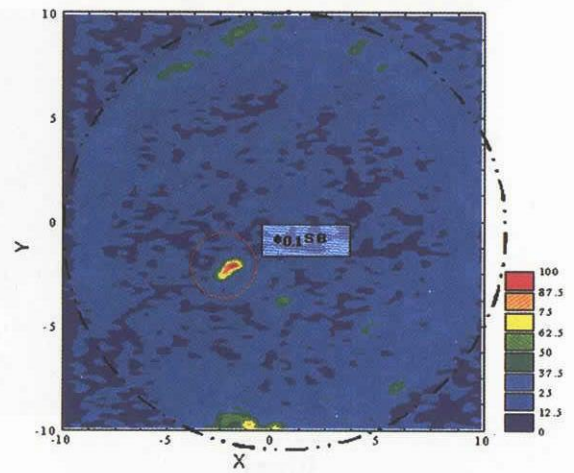

(b) ϕ 0.1 mm particle

Fig.4-16 Images of echo signal intensity detected by C-scan probe

5. CONCLUSION

(1) The experimental study on thermocapillary convection of low Prandtl number fluid was carried out to understand transition behavior to oscillatory flow. The half-zone liquid bridge of molten tin was formed between hot and cold disks in high vacuum chamber (10^{-5} Pa). The three radiation thermometers were used to measure the free surface temperature at a different azimuthal location at the same time. In addition, the temperature distribution at interface between liquid bridge and cold disk was measured by using very fine thermocouples to detect the transition point and to make clear the oscillation mode more precisely.

(2) It can be detected that the steady thermocapillary convection changes to oscillatory under certain condition. The observed phenomena of transition processes after the oscillatory onset were revealed by comparing to numerical result done by Imaishi *et al.*. The effect of aspect ratio (L/r) on critical Marangoni number was investigated. The critical Marangoni number decreases with increasing the aspect number. This behavior agrees with numerical simulation done by Imaishi *et al.* qualitatively except for region of smaller aspect ration.

(3) The surface tension and its temperature coefficient were measured in the experimental chamber. A molten tin droplet was formed on an α-Al_2O_3 substrate in the evacuated experimental chamber. These analog photo images were transfer to digital images and the surface tension was calculated from the outlines of digital image, which was the sessile drop method. The value of surface tension and its temperature coefficient were 520~550 [mN/m] and 0.097 [mN/m/K].

(4) The Fe-Ni/SB tracer particle has been developed for the visualization of the inner flow pattern of the Marangoni convection. Considering the traceability of the particle, high wettability and low reactivity with surrounding fluid, and high sphericity are required. Therefore, the multi-layer structure, which comprises Fe and Ni layers, was adopted. The plating techniques of both Fe and Ni layers were developed and the heat treatment technique to make the high sphericity particles was also developed. The test particle has already been manufactured and its reflectance of ultrasonic beam has been evaluated.

References

[1] H. Kuhlmann, in: Hydrodynamic Instabilities in Thermocapillary Flows, Microgravity Science Technology VII/2 (1994) 75.

[2] N. Imaishi, S. Yasuhiro, T. Sato, and S. Yoda, in: Proc. 44th SPIE Annual Meeting and Exhibition, Materials Research in Low Gravity II, Denver, **3792** (1999) 344.

[3] N. Imaishi, S. Yasuhiro, and S. Yoda, in: Marangoni Convection Modeling Research Annual Report (NASDA-TMR-000006E), National Space Development Agency of Japan (2000) 157.

[4] S. Nakamura, T. Hibiya, K. Kakimoto, N. Imaishi, S. Nishizawa, A. Hirata, K. Mukai, S. Yoda, and T. Morita, J. Crystal Growth, **186** (1998) 85.

[5] T. Hibiya, S. Nakamura, N. Imaishi, K. Mukai, K. Onuma, P. Dold, A. Cröll, K-W. Benz, and S. Yoda, in: Proc. Joint 1st Pan-Pacific Basin Workshop and 4th Japan-China Workshop on Microgravity Sciences, Tokyo (1998) 8.

[6] J. Han, Z. Sun, L. Dai, J. Xie, and W. Hu, J. Crystal Growth, **169** (1996) 129.

[7] Y.K. Yang and S. Kou, J. Crystal Growth, **222** (2001) 135.

[8] R. Imai, K. Takagi, M. Ohtaka, F. Ohtsubo, H. Natsui, and S. Yoda, in: Marangoni Convection Modeling Research Annual Report (NASDA-TMR-990007E), National Space Development Agency of Japan (1999) 71.
[9] K. Takagi, M. Ohtaka, H. Natsui, T. Arai, and S. Yoda, in: Marangoni Convection Modeling Research Annual Report (NASDA-TMR-000006E), National Space Development Agency of Japan (2000) 115.
[10] K. Takagi, M. Otaka, H. Natsui, T. Arai, S. Yoda, Z. Yuan, K. Mukai, S. Yasuhiro, and N. Imaishi, J. Crystal Growth, **233** (2001) 399
[11] M. Ohtaka, K. Takagi, H. Natsui, T. Arai, and S. Yoda, in: Proc. 2nd Pan-Pacific Basin Workshop on Microgravity Sciences, Pasadena (2001) IF-1159.
[12] K. Takagi, M. Otaka, H. Natsui, T. Arai, and S. Yoda, J. Jpn. Soc. Microgravity Appl. (in Japanese), **18** (2001) 11.
[13] N. Imaishi, S. Yasuhiro, Y. Akiyama and S. Yoda, J. Crystal Growth, **230** (2001) 164
[14] Z.Yuan, K.Mukai, K.Takagi and M.Ohtaka, J.Jpn. Inst. Metals (in Japanese), **65** (2001) 21.
[15] A. Passerone, E.Ricci and R.Sangiorgi, J. Material Sci., **25** (1990) 4266
[16] R.Sangiorgi, C.Senillou and J.C.Joud, Surface Sci., **202** (1988) 509